

BOW SHOCK AND RADIO HALO IN THE MERGING CLUSTER A520

M. MARKEVITCH^{1,2}, F. GOVONI³, G. BRUNETTI³, AND D. JERIUS¹

Submitted to *ApJ*, 2004 December 16

ABSTRACT

Chandra observations of the merging galaxy cluster A520 reveal a prominent bow shock with $M = 2.1^{+0.4}_{-0.3}$. This is only the second clear example of a substantially supersonic merger shock front in clusters. Comparison of the X-ray image with that of the previously known radio halo reveals a coincidence of the leading edge of the halo with the bow shock, offering an interesting experimental setup for determining the role of shocks in the radio halo generation. The halo in A520 apparently consists of two spatially distinct parts, the main turbulence-driven component and a cap-like forward structure related to the shock, where the latter may provide pre-energized electrons for subsequent turbulent re-acceleration. The radio edge may be caused by electron acceleration by the shock. If so, the synchrotron spectrum should have a slope of $\alpha \simeq 1.2$ right behind the edge with quick steepening further away from the edge. Alternatively, if shocks are inefficient accelerators, the radio edge may be explained by an increase in the magnetic field and density of pre-existing relativistic electrons due to gas compression. In the latter model, there should be radio emission in front of the shock with the same spectrum as that behind it, but 10–20 times fainter. If future sensitive radio measurements do not find such pre-shock emission, then the electrons are indeed accelerated (or re-accelerated) by the shock, and one will be able to determine its acceleration efficiency. We also propose a method to estimate the magnetic field strength behind the shock, based on measuring the dependence of the radio spectral slope upon the distance from the shock. In addition, the radio edge provides a way to constrain the diffusion speed of the relativistic electrons.

Subject headings: Galaxies: clusters: individual (A520) — intergalactic medium — X-rays: galaxies: clusters — Radio continuum

1. INTRODUCTION

Cluster mergers convert kinetic energy of the gas in colliding subclusters into thermal energy by driving shocks and turbulence in the gaseous halo of the merged cluster. A fraction of this energy may be diverted into nonthermal phenomena, such as magnetic field amplification and the acceleration of relativistic particles that manifest themselves via synchrotron radio halos (recently reviewed by, e.g., Feretti 2002, 2004; Kempner et al. 2004) and inverse Compton hard X-ray emission (e.g., Fusco-Femiano et al. 2004; Rephaeli & Gruber 2002). This energy fraction depends on microphysics of the magnetized intracluster plasma, which is poorly known. Shock fronts may provide a unique observational tool to study the above processes, because they create high-contrast features in the cluster X-ray images (and, as we shall see, in the radio images), and because they are those rare locations in clusters where gas velocities in the sky plane can be determined from the X-ray imaging spectroscopy (e.g., Markevitch, Sarazin, & Vikhlinin 1999).

Until recently, the only unambiguous cluster merger shock (exhibiting both a sharp gas density edge and a convincing temperature jump, the prerequisites for determining the gas velocity and density jumps) was that found by *Chandra* in 1E0657–56 (Markevitch et al. 2002). In this paper, we present the second such example discovered in A520, a merging cluster at $z = 0.203$. While many clusters exhibit merging and shock-heated gas, observations of shock *fronts* are so rare because one has to catch a merger at a very specific stage when the shock has not yet moved to the outer, low surface brightness regions, and at a sufficiently small angle from the

sky plane so that projection does not hide the density edge.

Both A520 and 1E0657–56 have radio halos (Govoni et al. 2001; Liang et al. 2000). Close relation between halos and mergers was extensively discussed (e.g., Feretti 2002; Buote 2001; Markevitch & Vikhlinin 2001; Govoni et al. 2004, hereafter G04). Merger-driven turbulence is likely the main process responsible for generation of the ultrarelativistic electrons producing the diffuse radio emission (e.g., Schlickeiser, Sievers, & Thiemann 1987; Brunetti et al. 2001; Fujita, Takizawa, & Sarazin 2003), but the contribution due to shock acceleration (e.g., Harris et al. 1980; Tribble 1993; Sarazin 1999) is still not clear. The best way to separate these two contributions is to look at a cluster with a bow shock and a radio halo, which is what we do in this paper.

We assume a flat cosmology with $H_0 = 70 \text{ km s}^{-1} \text{ Mpc}^{-1}$ and $\Omega_0 = 0.3$, in which $1''$ is 3.34 kpc at the cluster's redshift. Uncertainties are 90% unless stated otherwise.

2. X-RAY ANALYSIS

A520 was observed with *Chandra* ACIS-I twice. Results from the first, short (9 ks) exposure taken in October 2000 were presented in G04. In December 2003, the cluster was re-observed for 67 ks. We analyze this dataset here and omit the earlier exposure for simplicity. The data were prepared and cleaned in a standard manner; the instrument responses for spectral analysis were generated as described in Vikhlinin et al. (2004). The background was modeled using the blank-sky dataset as described in Markevitch et al. (2003b). We encountered a minor complication in the form of a slowly-varying 10% background excess over the quiescent level at $E < 8 \text{ keV}$, somewhat similar to (but smaller than) that described in Markevitch et al. (2002). In the image area free of cluster emission, and in the energy interval 0.8–9 keV that we used for spectral fitting, the spectrum of the excess was well-modeled by a power law with photon index -0.7 (with-

¹ Harvard-Smithsonian Center for Astrophysics, 60 Garden St., Cambridge, MA 02138; maxim@head.cfa.harvard.edu

² Space Research Institute, Moscow, Russia

³ Istituto di Radioastronomia del CNR, Bologna, Italy

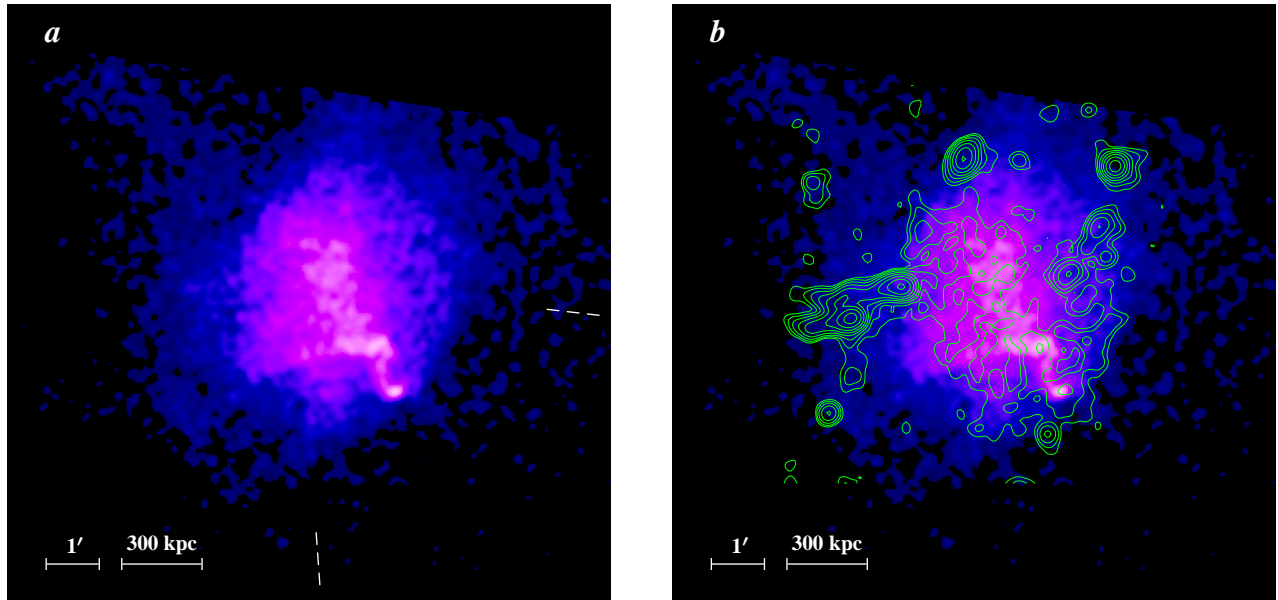


FIG. 1.— (a) ACIS 0.5–2 keV image of A520 smoothed with a $\sigma = 4''$ Gaussian. Point sources are removed. A bow shock is propagating in the SW direction from the cluster center. Dashed lines mark a sector used for radial profiles across the shock shown in Fig. 2. (b) VLA 1.4 GHz contours from Govoni et al. (2001) overlaid on the X-ray image. Discrete sources not related to the diffuse emission are not removed from the radio image. FWHM is $15''$; contours are spaced by a factor of 2.

out applying the mirror effective area or CCD efficiency to the model). We assumed this component to be spatially uniform and included it in the fits. The uncertainty of this component propagates into errors of best-fit temperatures that are smaller than the statistical errors for the interesting cluster regions.

Fig. 1a shows a smoothed ACIS image of the cluster. As seen from the X-ray as well as weak lensing data (Clowe et al. in prep.), the cluster undergoes a merger along the NE-SW direction. A bright irregular structure southwest of center consists of dense, cool pieces of a cluster core that has been broken up by ram pressure as it flew in from the NE direction (Markevitch et al. in prep). In front of this structure is a prominent bow-shaped brightness edge perpendicular to the merger direction. This was suggested by the earlier, shorter, exposure; the new observation provides sufficient statistics to determine that it is a shock front.

Fig. 2a shows a radial brightness profile across this edge, extracted in a sector marked in Fig. 1a and excluding regions affected by the dense core structures. The energy band 0.5–2 keV was chosen to minimize the dependence of the X-ray brightness on temperature. The profile has the characteristic shape of a projected sharp spherical density discontinuity. We therefore fit it with such a radial density profile (two power laws with a jump), shown in panel b and in projection as a histogram in panel a. The best-fit amplitude of the density jump, after a small (3%) correction for the measured temperature difference across the edge, is $x \equiv \rho_2/\rho_1 = 2.3 \pm 0.3$. The gas temperatures in the same sector are $T_1 = 4.8^{+1.2}_{-0.8}$ keV and $T_2 = 11.5^{+6.7}_{-3.1}$ keV for the low and high density side of the edge, respectively. The latter temperature value is “deprojected”, for which we used the best-fit density model to subtract the (small) contribution of the outer cooler gas on the line of sight near the shock.

The sign of the temperature jump confirms that the edge is indeed a shock front. From the Rankine-Hugoniot shock conditions, we can use the above density and temperature

jumps to obtain two independent estimates of its Mach number. They are $M = 2.1^{+0.4}_{-0.3}$ and $2.2^{+0.9}_{-0.5}$, respectively, in good mutual agreement; we will use the more accurate value from the density jump. From the gas temperatures and the Mach number, the velocities of the pre-shock and post-shock gas flows in the shock reference frame are approximately 2300 km s^{-1} and 1000 km s^{-1} , respectively.

3. DISCUSSION

3.1. Radio edge

A520 has a prominent radio halo (Govoni et al. 2001), whose brightness contours are overlaid on the X-ray image in Fig. 1b. G04 already noted a remarkable coincidence of the SW edge of the radio halo with the shock-like X-ray feature, although at that time it was not clear whether the feature is a shock front. A similar extension of the radio halo edge to the bow shock is seen in 1E 0657–56 (Markevitch et al. 2002; G04). In another merging cluster, A665, a “leading” edge of the halo also corresponds to a region of hot gas that is probably behind a bow shock, although the X-ray image of A665 does not show a gas density edge at the shock, probably due to an unfavorable viewing angle (Markevitch & Vikhlinin 2001; G04). The overall structure of the halo in A520 may even suggest two distinct components, a mushroom with a stem and a cap, where the main stem component goes across the cluster and the cap ends at the bow shock. The main component appears to be in the region of the cluster where one expects relatively strong turbulence (G04). In this paper, we concentrate on the halo edge.

3.1.1. Shock acceleration

One possible explanation for the radio edge is acceleration of electrons to ultrarelativistic energies by the shock. The shock should generate electrons with an energy spectrum

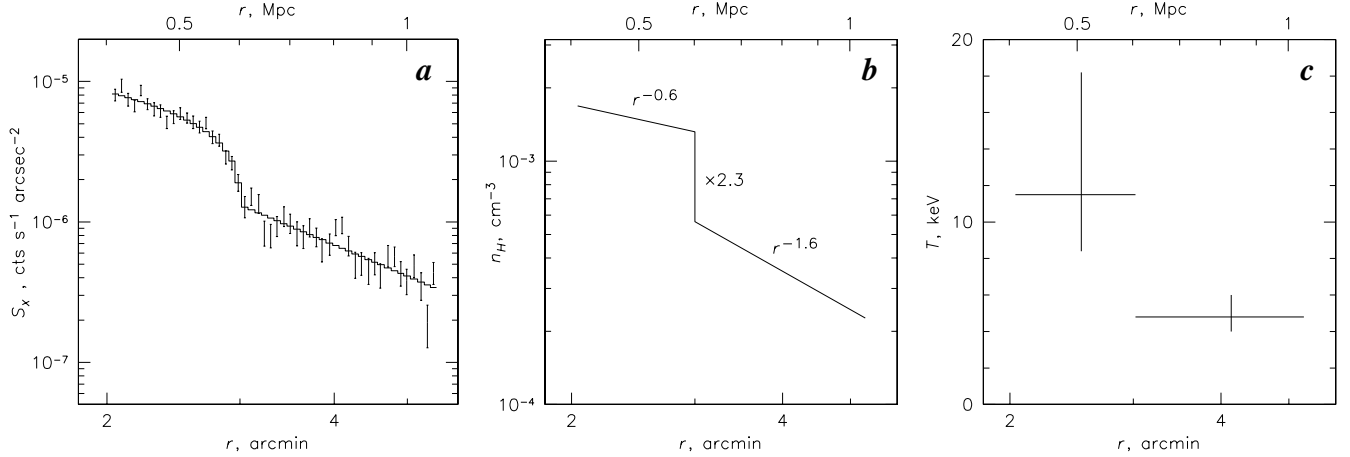


FIG. 2.— (a) The 0.5–2 keV brightness profile across the bow shock in a sector marked in Fig. 1a (see text). Errors here are 1σ ; histogram shows the best-fit model whose radial density profile is given in panel (b). (c) Temperatures across the shock (errors are 90%). The r axis shows a distance from the shock’s center of curvature, which is near the centroid of the cluster.

$dN/d\gamma = N_0\gamma^{-p}$ with

$$p = \frac{x+2}{x-1} \quad (1)$$

via first-order Fermi acceleration (e.g., Blandford & Eichler 1987); $p \simeq 3.3$ for our shock with $x \simeq 2.3$. The synchrotron emission should have a spectrum $I_\nu \propto \nu^{-\alpha}$ with $\alpha = (p-1)/2 \simeq 1.2$ right behind the shock front. However, these electrons are short-lived because of IC and synchrotron energy losses, and their spectrum will quickly steepen. The respective electron lifetimes, t_{IC} and t_{syn} , are

$$t_{IC} = 2.3 \times 10^{12} \gamma^{-1} (1+z)^{-4} \text{ yr} \quad (2)$$

and

$$t_{syn} = 2.4 \times 10^{13} \gamma^{-1} \left(\frac{B}{1 \mu G} \right)^{-2} \text{ yr} \quad (3)$$

(e.g., Sarazin 1999). IC losses dominate for $B < 3 \mu G$; other losses are negligible for our range of energies and fields. For a power-law electron spectrum with $p = 2-4$ (expected for shocks with $M > 1.7$), the contribution of different γ at a given synchrotron frequency has a peak at

$$\gamma_{peak} \approx 10^4 \left(\frac{\nu}{1 \text{ GHz}} \right)^{1/2} \left(\frac{B}{1 \mu G} \right)^{-1/2}. \quad (4)$$

The exact value depends only weakly on p in the interesting range, and the emission at a given frequency comes from a relatively narrow interval of γ . Assuming $B \sim 1 \mu G$, the lifetime for electrons with $\gamma \sim 1.2 \times 10^4$ that emit at 1.4 GHz in A520 is $\sim 10^8$ yr. Thus, given the 1000 km s^{-1} velocity of the downstream flow (§2) that carries these electrons away from the shock, the width of the synchrotron-emitting region should only be about 100 kpc, beyond which the electrons cool out of the 1.4 GHz band. At lower frequencies, the cooling is slower and this region will be wider (we discuss this in more detail in §3.2). This scale is an order of magnitude smaller than the size of the halo, so the whole halo cannot be produced by particles accelerated at this shock. This is true for merger shocks in general (e.g., Brunetti 2003). However, the cap-like part of the radio halo appears to have just the right width, $\Delta r \lesssim 100$ kpc (considering the finite angular resolution). Thus with the available data, this region is not inconsistent with shock acceleration and may be a “radio gischt”, using the classification of

Kempner et al. (2004). While the relativistic particles in this structure cool down soon after the shock passage, some may later be picked up and re-accelerated as they reach the turbulent region behind the subcluster core, where the stem-like halo component forms.

3.1.2. Compression of fossil electrons

However, the efficiency with which collisionless shocks in clusters can accelerate particles is unknown, and may be insufficient to generate the observed radio brightness. The radio edge in A520 offers an interesting prospect for constraining it. If the acceleration efficiency is low, the observed radio edge may alternatively be explained by an increase in the magnetic field strength and the energy and density of the pre-existing relativistic electrons simply due to the gas compression at the shock. Such pre-existing particles may be, for example, secondary electrons generated by relativistic protons (e.g., Denison 1980) or cooled primary electrons accumulated from previous merger events (e.g., Sarazin 1999). This is similar to the scenario proposed by Enßlin & Gopal-Krishna (2001) for radio relics, which may be regions of fossil radio plasma re-energized by a recent merger shock passage. In this model, the pre-existing electrons must produce diffuse radio emission *in front of* the bow shock, whose intensity and spectrum may be predicted from the shock compression factor and the post-shock radio spectrum, as given below.

For a rough estimate, we assume that as the gas crosses the shock surface, its tangled magnetic field is compressed isotropically (indeed, observations at the Earth’s bow shock show that a shock passage strengthens the field whether it is parallel or perpendicular to the shock, e.g., Wilkinson 2003 and references therein). The average field strength B then increases by a factor

$$B \propto x^{2/3} \quad (5)$$

(and the energy density as $x^{4/3}$), where x is the gas density jump. We further assume for simplicity that relativistic particles do not have a significant velocity component along the field lines. This shouldn’t be too far from the truth, because in a highly nonuniform field, the particles spend most of their time in the field bottlenecks and mirrors where the component of their momentum perpendicular to the field indeed dominates. The shock passage would then cause the particles to

spin up as $\gamma \propto B^{1/2}$ (the adiabatic invariant). For a power-law fossil electron spectrum of the form

$$dN/d\gamma = N_0 \gamma^{-\delta}, \quad (6)$$

such a shift in energy would preserve the slope of the spectrum and increase its normalization proportional to $B^{(\delta-1)/2}$. In addition, the number density of relativistic electrons increases by another factor of x due to the compression, so the electron spectrum normalization after the shock passage will change as (given eq. 5)

$$N_0 \propto x^{(\delta+2)/3}. \quad (7)$$

(Note that we recover the relativistic adiabat for the particles: across the shock, their volume energy density changes as $P \propto x\gamma \propto x^{4/3}$.) For a power-law electron spectrum, the synchrotron surface brightness at a given frequency is $I_\nu \propto \int N_0 B^{(\delta+1)/2} dl$, where the integral is along the line of sight. For our viewing geometry with the shock surface parallel to the line of sight, it should exhibit a jump at the shock

$$I_\nu \propto x B^\delta \propto x^{\frac{2}{3}\delta+1}. \quad (8)$$

Thus, for our shock with $x = 2.3$, if the radio edge is due to the compression only, there must be a pre-shock radio emission with the same spectrum as post-shock but fainter by a factor of 12–20 for $\delta = 3–4$, respectively (in practice, δ can be determined from the post-shock radio spectrum).

The assumption of a power law spectrum can be relaxed somewhat. The frequency at which the particle emits most of its synchrotron radiation scales across the density jump as

$$\nu_{\text{peak}} \propto B \gamma^2 \propto x^{4/3}, \quad (9)$$

or by a factor of 3 for the A520 shock. Even if the spectrum deviates from a pure power law, the pre-shock spectrum can still be predicted directly from the post-shock spectrum at the frequencies scaled down as given above.

Given the simplifying assumptions about the change of the magnetic field and particle energy at the shock, the above is of course only a rough estimate, but it should not be too far off. One can obtain estimates within a factor of 2 for the I_ν increase under very simple alternative assumptions about the field structure.

3.1.3. Re-acceleration of fossil electrons

In addition to the two mechanisms discussed above, there is a third possibility, namely, re-acceleration of the fossil electrons by the shock. In the linear acceleration regime, the post-shock electron spectrum will be (e.g., Blandford & Eichler 1987):

$$N(\gamma) = (p+2)\gamma^{-p} \int_{\gamma_{\text{min}}}^{\gamma} N_f(\gamma') \gamma'^{p-1} d\gamma', \quad (10)$$

where p is from eq. (1), γ_{min} is the minimum energy of the particles that are accelerated at the shock (or present in the fossil population, whichever is higher), and $N_f(\gamma)$ is the fossil electron spectrum. If the latter is a power law given by eq. (6), and is steeper than the one produced by direct shock acceleration (i.e., $\delta > p$), the post-shock spectrum will acquire the slope p and its normalization will increase by a large factor dependent on γ_{min} . In practice, this case will probably be indistinguishable from direct shock acceleration considered above. If the fossil spectrum is flatter with $\delta < p$, the post-shock spectrum will preserve the slope δ while its normalization will increase as

$$N_0 \propto \frac{3x}{x+2-\delta(x-1)}. \quad (11)$$

A comparison of this factor to the one derived for the compression (eq. 7) confirms the intuitive expectation that re-acceleration would provide a bigger boost to the fossil electron spectrum than simple compression. For example, for $\delta = 2–3$, an increase due to the compression is by factors of $\approx 3–4$ for our shock, while the re-acceleration increase is by factors of $\approx 4–17$, respectively. We should note that a boost of the fossil electron spectrum due to the magnetic field compression should occur regardless of the presence of shock acceleration, but whether or not these two effects are additive probably depends on the exact processes on the microscopic level. The magnetic field should increase across the shock by the same amount in all three scenarios.

3.1.4. Observational prospects

The above estimates show that the least efficient way to create the radio edge is the increase of the energy of the pre-existing relativistic electrons due to the compression of the magnetic field by the shock. In such a scenario, those fossil electrons should generate synchrotron emission in front of the shock. If future sensitive measurements do not detect a pre-shock radio emission at the level predicted for simple compression, it would mean that the shock generates relativistic electrons and/or a magnetic field, as opposed to simply compressing them. Observations of interplanetary shocks of a similar strength and high thermal-to-magnetic pressure ratio relevant for cluster plasma seem to be consistent with a simple compression of the field (Russell & Greenstadt 1979), so magnetic field generation is unlikely. Thus such a non-detection would provide a direct estimate of the shock's particle acceleration efficiency.

While the expected pre-shock emission may be below the current measurement sensitivity, one can get an initial idea of the origin of the electrons in the cap of the halo by measuring the radio spectrum immediately behind the edge. If the electrons are shock-accelerated directly, the radio spectral slope should be $\alpha = 1.2$. Within the range of possibilities that we have considered, a steeper spectrum would point to compressed fossil electrons, and a flatter spectrum would indicate fossil electrons with a flat initial energy spectrum, either compressed or re-accelerated.

Because the bow shock is spatially separated from the turbulent area further downstream (except for the region around the small dense core fragments) and there is no reason to expect significant turbulence and additional acceleration in that intermediate region, the cap-like structure is likely to exhibit a measurable spectral difference from the main halo. Within the 100 kpc-wide strip along the shock, the spectrum should quickly steepen starting from $\alpha = 1.2$ (or other, probably not very different, value as discussed above). If the region is unresolved, the resulting mixture would have a volume-averaged slope $\bar{\alpha} \approx \alpha + 1/2$ (Ginzburg & Syrovatskii 1964) which is significantly steeper than $\alpha \approx 1–1.2$ observed on average in most halos (e.g., Feretti 2004), the bulk of which is probably continuously powered by turbulence. Interestingly, Feretti et al. (2004) found that the presumed post-shock region in A665 indeed exhibits the steepest radio spectrum in the spectral index map of the cluster, which is consistent with the above two-component cap + stem picture.

3.2. Magnetic field estimate

Regardless of the exact origin of the relativistic electrons responsible for the radio edge, the distinct “gischt” in A520,

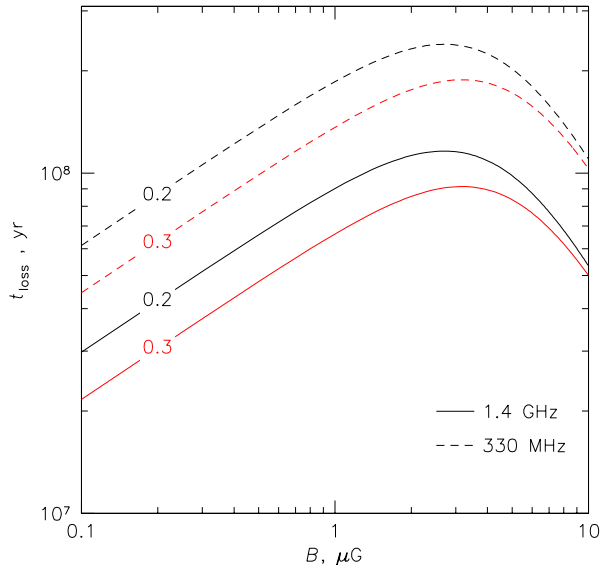


FIG. 3.— Lifetime of the relativistic electrons that contribute the most to the synchrotron emission at a certain frequency, for a $p = 3-4$ electron spectrum, as a function of B . Two frequencies are shown as solid and dashed lines. Black and red lines correspond to two different redshifts ($z = 0.2$ for A520 and $z = 0.3$ for 1E 0657–56).

and perhaps a similar region in 1E 0657–56, provide an interesting possibility for estimating the magnetic field strength behind the shock. As discussed above, IC and synchrotron cooling cause the electron spectrum to steepen and the electrons to drop out of the radio image on timescales of order 10^8 yr. This timescale depends on B as shown in Fig. 3, which combines eqs. (2, 3, 4). It gives the lifetime of the electrons that contribute the most at a given frequency, for a $p = 3-4$ spectrum and an interesting range of B . We assume that the bow shock causes a momentary increase in electron energy and B . The post-shock gas flows away from the shock with a known velocity and effectively “unrolls” the time evolution of the electron spectrum along the spatial coordinate (assuming no diffusion, see §3.3, and neglecting for this simple estimate the change of the post-shock velocity with coordinate). Thus the width of the “gischt”, if it is resolved, can give us the measure of the magnetic field. In practice, such a measurement needs to be done at more than one frequency in order to determine the spectrum of the electrons for a more precise calculation of γ_{peak} (and of course to verify that the electrons cool as predicted at different frequencies, that is, no acceleration occurs after the shock passage). In addition, the radio angular resolution has to be sufficient to perform at least a rough deprojection of the spherical edge of the bow shock (cf. Figs. 2a,b) and exclude the (possibly turbulent) region around the dense core remnant (Fig. 1a). A cooling time 2×10^7 yr (the minimum interesting time) corresponds to the $6''$ distance from the front, which gives the minimum resolution requirement. The available single-frequency radio data (Fig. 1b) do not have the needed signal to noise ratio or resolution, but are not inconsistent with B of order a μG . Such a measurement may be easier in 1E 0657–56 than in A520, as the shock there is more prominent and farther away from the turbulent area.

This method is reminiscent of that of Harris & Romanishin (1974) which compares the hard X-ray IC and radio synchrotron luminosities, in that it also combines the IC and synchrotron emission. The field values derived from the

IC/synchrotron ratio have persistently been lower than those derived from Faraday rotation (see Carilli & Taylor 2002 for a review). One of the proposed explanations is that the hard X-ray and radio emissions come from different electron populations in regions with different fields (e.g., Rudnick 2000). Our method would be free from this complication, because we essentially estimate the IC losses using the time evolution of the synchrotron emission from exactly the same electrons. Our method can distinguish among the values in the controversial interval of $B \sim 0.1-3 \mu\text{G}$, although, as seen from Fig. 3, it cannot give an unambiguous value of B . Note also that the magnetic field behind the shock would be amplified as discussed in §3.1.2.

3.3. Diffusion of relativistic particles

The above argument assumes that relativistic particles do not diffuse through the gas away from their place of origin. Diffusion with a velocity less than the 1000 km s^{-1} shock velocity would not alter the picture qualitatively. The diffusion speed is not expected to exceed the Alfvén velocity of $\approx 50 (B/1 \mu\text{G}) \text{ km s}^{-1}$ (e.g., Jaffe 1977), because faster-diffusing particles should be slowed down by self-generated Alfvén waves. If in reality this mechanism is not effective and the diffusion is much faster, a factor of $M = 2.1$ or more above the sound speed, it will spread the radio edge into the pre-shock region. Therefore, the study of the radio edge also provides an interesting opportunity to detect or place a direct limit on the diffusion of relativistic particles.

4. SUMMARY

The *Chandra* observation of A520 reveals a prominent bow shock with $M = 2.1$, which is only the second clear example of a substantially supersonic merger shock front besides 1E 0657–56. The shock coincides with an apparent leading edge of the radio halo. In light of this coincidence, we discuss possible explanations for the radio edge, which include direct acceleration of relativistic electrons by the shock, or energizing pre-existing electrons via shock re-acceleration or the compression of the magnetic field. Both models make testable predictions. In particular, the compression model predicts the existence of pre-shock radio emission at a level about 1/10–1/20 of the post-shock brightness. If one determines which of the models is valid, it could provide a measure of the particle acceleration efficiency in the cluster merger shocks. The slope of the radio spectrum immediately inside the edge may also give an idea of the nature of the edge, and possibly even test the applicability of the Fermi acceleration mechanism.

Regardless of the nature of the radio edge, it offers an interesting tool to measure the magnetic field strength in the post-shock gas (albeit not unambiguously) and exclude high rates of diffusion of the relativistic electrons, provided high-resolution radio data. All these measurements rely on the knowledge of the shock velocity and compression factor obtained from the X-ray. The shock fronts in A520 and 1E 0657–56 can thus provide unique information on the microphysics of the intracluster gas.

We thank Pasquale Blasi, Tracy Clarke, Alexey Vikhlinin and Dan Harris for stimulating discussions. Support for this work was provided by NASA contract NAS8-39073, *Chandra* grants GO2-3164X and GO3-4172X, and by INAF grant D4/03/15.

REFERENCES

- Blandford, R. & Eichler, D. 1987, *Phys. Rep.*, 154, 1
- Brunetti, G., Setti, G., Feretti, L., & Giovannini, G. 2001, *MNRAS*, 320, 365
- Brunetti G., 2003, Proc. "Matter and Energy in Clusters of Galaxies", Taiwan, ASP Conf. Series, eds. S. Bowyer & C.-Y. Hwang, 301, 349 (astro-ph/0208074)
- Buote, D. A., 2001, *ApJ*, 553, L15
- Carilli, C. L. & Taylor, G. B. 2002, *ARA&A*, 40, 319
- Dennison, B. 1980, *ApJ*, 239, L93
- Enßlin, T. A. & Gopal-Krishna 2001, *A&A*, 366, 26
- Feretti, L. 2002, *IAU Symposium*, 199, 133 (astro-ph/0006379)
- Feretti, L. 2004, astro-ph/0406090
- Feretti, L., Orrù, E., Brunetti, G., Giovannini, G., Kassim, N., & Setti, G. 2004, *A&A*, 423, 111
- Fujita, Y., Takizawa, M., & Sarazin, C. L., 2003, *ApJ*, 584, 190
- Fusco-Femiano, R., Orlandini, M., Brunetti, G., Feretti, L., Giovannini, G., Grandi, P., & Setti, G. 2004, *ApJ*, 602, L73
- Ginzburg, V. L. & Syrovatskii, S. I. 1964, *The Origin of Cosmic Rays* (New York: Macmillan)
- Govoni, F., Feretti, L., Giovannini, G., Böhringer, H., Reiprich, T.H., & Murgia, M., 2001, *A&A*, 376, 803
- Govoni, F., Markevitch, M., Vikhlinin, A., VanSpeybroeck, L., Feretti, L., & Giovannini, G. 2004, *ApJ*, 605, 695 (G04)
- Harris, D. E. & Romanishin, W. 1974, *ApJ*, 188, 209
- Harris, D. E., Kapahi, V. K., & Ekers, R. D. 1980, *A&AS*, 39, 215
- Jaffe, W. J. 1977, *ApJ*, 212, 1
- Kempner, J. C., Blanton, E. L., Clarke, T. E., Enßlin, T. A., Johnston-Hollitt, M., & Rudnick, L. 2004, in *The Riddle of Cooling Flows*, eds. T. Reiprich, J. Kempner, & N. Soker (astro-ph/0310263)
- Liang, H., Hunstead, R. W., Birkinshaw, M., & Andreani, P. 2000, *ApJ*, 544, 686
- Markevitch, M., Gonzalez, A. H., David, L., Vikhlinin, A., Murray, S., Forman, W., Jones, C., & Tucker, W. 2002, *ApJ*, 567, L27
- Markevitch, M., Sarazin, C. L., & Vikhlinin, A. 1999, *ApJ*, 521, 526
- Markevitch, M., & Vikhlinin, A., 2001, *ApJ* 563, 95
- Markevitch, M., et al., 2003, *ApJ*, 583, 70
- Rephaeli, Y. & Gruber, D. 2002, *ApJ*, 579, 587
- Rudnick, L. 2000, in *Cluster Mergers and their Connection to Radio Sources*, 24th meeting of the IAU, JD10, E22
- Russell, C. T. & Greenstadt, E. W. 1979, *Space Science Reviews*, 23, 3
- Sarazin, C. L. 1999, *ApJ*, 520, 529
- Schlickeiser, R., Sievers, A., & Thiemann, H., 1987, *A&A*, 182, 21
- Tribble, P. 1993, *MNRAS*, 263, 31
- Vikhlinin, A., Markevitch, M., Murray, S., Jones, C., Forman, W., & VanSpeybroeck, L. 2004, *ApJ*, submitted (astro-ph/0412306)
- Wilkinson, W. P. 2003, *Planet. Space Sci.*, 51, 629